Luminescence-Based Transcutaneous Carbon Dioxide Sensor IC using Dual-Lifetime Referencing

Tuna B. Tufan, Benjamin Larkin, John McNeill, Ulkuhan Guler
Dept. of Electrical and Computer Engineering, Worcester Polytechnic Institute, Worcester, MA, USA

***Abstract*—This work presents a first-of-its-kind integrated transcutaneous carbon dioxide sensing system, implemented in a standard 180 nm CMOS process, utilizing the time-domain dual lifetime referencing method. The system incorporates an opampless delta-sigma modulator-based direct current-to-digital converter to capture the luminescence response of a carbon dioxide-sensitive film. To improve accuracy, we propose a current scaling technique that dynamically adjusts the delta-sigma modulator's feedback current in response to variations in the photodiode current, which reflect changes in carbon dioxide partial pressures. This approach reduces conversion errors and prevents the delta-sigma modulator from saturation. The system achieves a resolution of 0.15nA/cnt while maintaining ∼0.5% mean calculation error across a 30 μA input range. We validated the system design through measurements in a gas chamber with carbon dioxide pressures ranging from 0 to 76 mmHg, covering the physiologically relevant range, as well as in a human subject where it successfully captured a hyperventilation event.**

***Index Terms*—Carbon dioxide sensor, transcutaneous sensing, partial pressure of carbon dioxide, dual lifetime referencing, luminescence sensing, wearable, ventilation, respiration.**

I. Introduction

Respiration is a vital physiological process, and its effectiveness is closely tied to the regulation of carbon dioxide (CO_2) levels in the blood. The partial pressure of CO_2 in arterial blood ($PaCO_2$) reflects the dynamic balance between metabolic CO_2 production and pulmonary clearance, making it a key biomarker for respiratory health. Accurate assessment of $PaCO_2$ is crucial for diagnosing and managing respiratory conditions such as chronic obstructive pulmonary disease (COPD), sleep apnea, and acute respiratory failure [1].

Traditionally, $PaCO_2$ has been measured invasively through blood samples or noninvasively using methods that are limited to intubated patients [2] or restricted to bulky bedside devices typically found in intensive care units [3]. These traditional approaches are inadequate for continuous, remote monitoring in ambulatory or at-risk populations. Enabling real-time, non-invasive, wearable CO_2 monitoring could transform the management of respiratory conditions by offering a path toward more personalized, proactive, and accessible healthcare.

Recent advancements in luminescence sensing have enabled the development of compact wearable devices capable of measuring CO_2 molecules diffusing through the skin, i.e., transcutaneous CO_2 sensing [4], which is directly correlated with $PaCO_2$. These devices offer continuous and unobtrusive CO_2 monitoring, allowing users to maintain their daily activities while supporting remote healthcare. However, miniaturized wearable CO_2 sensors are exceptionally rare, with only a few examples reported to date [5], [6], [7]. Among these, [5], [6] use near-infrared sensing, which suffers from trade-offs between device size and detection resolution, limiting device miniaturization. Meanwhile, [7] employs luminescence sensing but is limited to a proof-of-concept stage prototype using off-the-shelf components. To date, none of the approaches have advanced to an IC-level implementation.

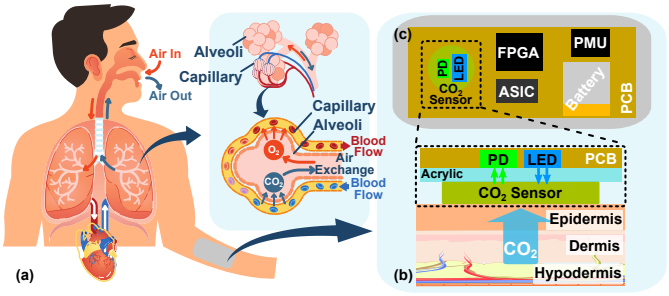

Fig. 1. (a) Cardiopulmonary gas exchange, (b) CO_2 sensor capturing CO_2 molecules diffused through the skin, and (c) the conceptual transcutaneous carbon dioxide monitoring wearable.

This work presents an initial step toward creating a wearable for continuous and remote monitoring of transcutaneous CO_2 by introducing the first integrated luminescence-based sensing system, illustrated conceptually in Fig.1. The design, implemented in a 180 nm CMOS process, utilizes the time-domain dual lifetime referencing (t-DLR) technique [8]. The proposed system demonstrates several key features: 1) a $\Delta\Sigma$ modulator based front end with direct charge-to-digital conversion, eliminating the need for a transimpedance amplifier (TIA); 2) an I-DAC-based current scaling technique, improving the conversion accuracy while eliminating the need for multiple comparators; and 3) resolution required to sense partial pressure of CO_2 (PCO_2) as low as 3.8 mmHg, lower than Food and Drug Administration requirements. 4) Canceling errors caused by confounding factors often requires additional reference circuitry. In contrast, proposed approach uses a single detector and signal path for both luminescence detection and processing, while still effectively eliminating errors from confounding influences. The system's functionality and robustness are demonstrated repeatedly 5) by measuring PCO_2 in both a gas chamber and a human subject, effectively capturing a hyperventilation event. The rest of the paper is structured as follows. Section II covers the fundamentals of time-domain dual lifetime referencing, Section III describes the system

This material is based upon work in part supported by the National Science Foundation (NSF) under Grant ECCS-2143898 and the National Institute of Health (NIH) under Grant NIBIB-R21EB036329. Corresponding author: Ulkuhan Guler: uguler@wpi.edu.

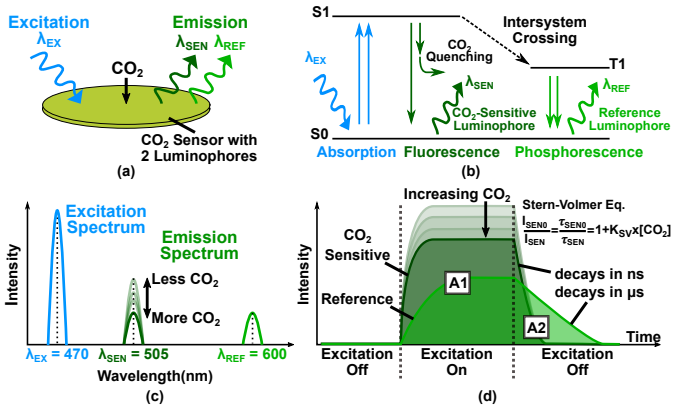

Fig. 2. (a) CO_2 sensor, (b) simplified electronic state diagram, (c) CO_2 sensor's luminescence spectra, and (d) time-domain luminescence response.

architecture, Section IV demonstrates the measurement results, and Section V concludes the paper.

II. Time-Domain Dual Lifetime Referencing

The system measures CO_2 employing a luminescent film (CO_2 sensor) illustrated in Fig.2.a. When excited by blue light, the luminophores, which are atomic groups in the CO_2 sensor, transition from the ground state (S0) to a higher energy electronic state (S1), as demonstrated in the simplified electronic state (Jablonski) diagram in Fig.2.b. Some luminophores return directly to S0, emitting a photon at a longer wavelength than the excitation wavelength with lower energy; this process is known as fluorescence. The intensity and lifetime of this emission, where the lifetime typically falls in the nanoseconds range, are influenced by PCO_2. As a result, these luminophores are referred to as CO_2-sensitive. Other luminophores transition to the first triplet state (T1) before returning to S0, emitting photons at longer wavelengths in a process called phosphorescence. The intensity and lifetime of these luminophores, where the lifetime falls in the microsecond range, remain unaffected by CO_2, and thus we refer to them as reference luminophores. The emissions from both types of luminophores are collectively referred to as luminescence. The luminescence spectra of the CO_2 sensor is demonstrated in Fig.2.c.

Changes in PCO_2 can be detected by observing variations in the intensity (I_{SEN}) or lifetime (τ_{SEN}) of the CO_2-sensitive luminophores compared to their initial intensity (I_{SEN0}) and lifetime (τ_{SEN0}) when CO_2 is absent, as described by the Stern-Volmer equation shown in Fig.2.d. Intensity-based measurements are susceptible to confounding factors such as optical path variations and excitation strength, reducing reliability. In contrast, lifetime-based methods offer greater robustness to these factors, resulting in more accurate and consistent measurements [9]. However, they demand specialized optics and high-speed electronics to resolve the luminophores' nanosecond-scale lifetimes [4].

To overcome these challenges, we employ the t-DLR approach. The time-domain response of the luminophores, shown in Fig.2.d, indicates that the CO_2-sensitive and reference luminophores emit similar levels of luminescence during excitation. However, once the excitation ends, the reference luminophore's longer decay dominates since the CO_2-sensitive luminophore decays in nanoseconds. Due to the characteristics of these luminophores, the total luminescence during excitation (A1) depends on both excitation strength and PCO_2. The total luminescence after excitation (A2) depends only on the excitation strength, as the contribution from the CO_2-sensitive luminophore is negligible in that region. Because both luminophores are equally exposed to external influences, the ratio of A1 to A2 effectively cancels them out, ensuring a reliable and accurate measurement of CO_2 concentration. A detailed analysis of the t-DLR method and derived luminescence ratio (LR) is provided in [7]. The t-DLR method allows the luminescence to be captured and processed with a single detector and signal pathway, eliminating the need for additional reference circuits to cancel out external influences.

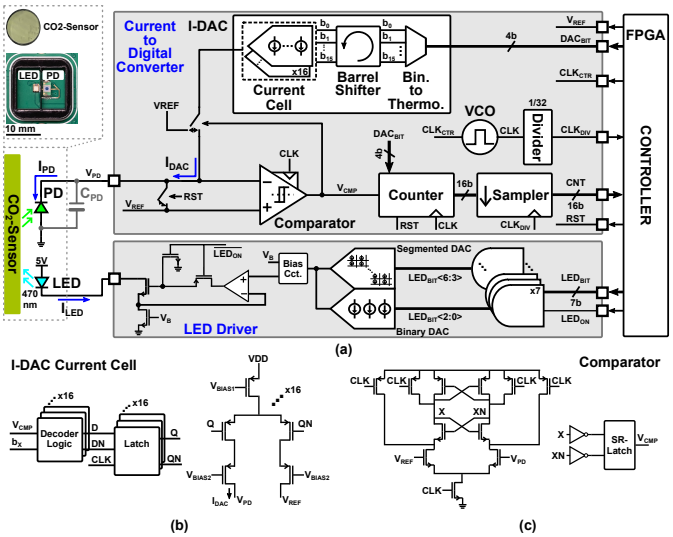

Fig. 3. (a) IC system diagram, schematic of (b) the I-DAC current cell and (c) the comparator.

III. System Architecture

Traditional optical front ends employ a cascaded topology, where an opamp-based TIA converts photocurrent into voltage, followed by an analog-to-digital converter (ADC) [10]. However, the limited bandwidth of the opamp can cause performance issues, such as accurately detecting the lifetime of the luminescence [11], leading to a degradation in measurement resolution. We set a resolution goal about two times more precise than the regulatory requirement for bedside transcutaneous CO_2 monitors [12], and equivalent to a 0.5% error in the LR value. Our simulations indicate a clock period of 3 ns for 0.5% error; hence, we opted for a high-speed, opamp-less current-to-digital converter (C2D) topology. The CO_2 sensing system is composed of two main subsystems: the C2D and the LED driver, depicted in Fig.3.a. The LED driver is designed to excite the CO_2 sensor with adjustable optical power, allowing for adaptation to various monitoring scenarios. The brightness of the LED is controlled via an

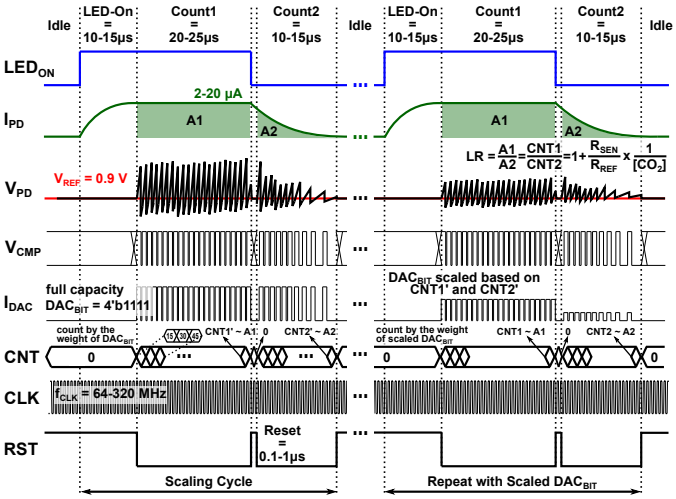

Fig. 4. System timing diagram.

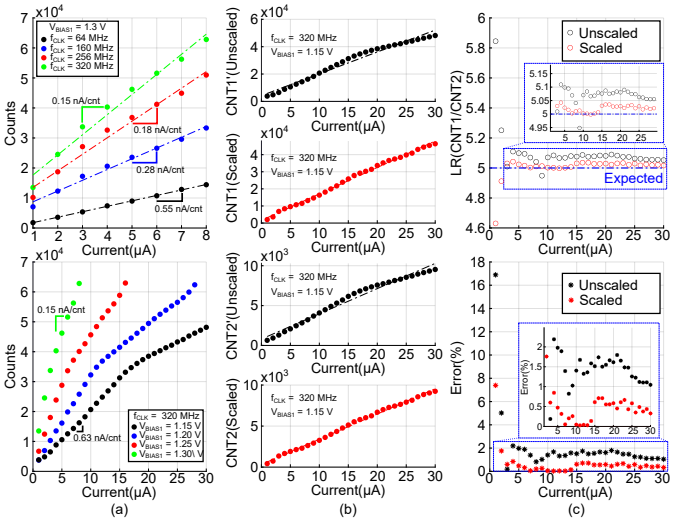

Fig. 5. (a) Resolution characterization with fixed V_{BIAS1} and varying f_{CLK} (top), varying V_{BIAS1} and fixed f_{CLK} (bottom), (b) counter outputs with scaled and unscaled I-DAC, (c) corresponding LR and system error.

integrated 7-bit DAC, regulated by control ($LED_{BIT<6:0>}$) and LED_{ON} signals provided by the FPGA.

In the proposed C2D circuit, the CO_2 sensor's luminescence is detected by a photodiode (PD). The generated photocurrent, I_{PD}, shifts the biasing point (V_{PD}) of the PD. To stabilize V_{PD}, the I-DAC injects current into the junction capacitance (C_{PD}) in response to the dynamic changes in the CO_2 sensor's luminescence. The I-DAC is controlled by 4-bit DAC_{BIT} signals from the FPGA, which are converted from binary to thermometer code. A barrel shifter is employed to mitigate the deterministic errors by rotating bits, thereby preventing cumulative inaccuracies. The barrel-shifted code is subsequently fed into the unit DAC cells to create the I_{DAC} current. A StrongArm comparator regulates the injected current by controlling the I-DAC switch based on the comparison of V_{PD} with a reference voltage (V_{REF}). The comparator output (V_{CMP}), representing the number of current injections proportional to the photocurrent, is counted by a 16-bit synchronous counter. This count is downsampled to align with the post-processing clock rate (CLK_{DIV}). A voltage-controlled oscillator (VCO) generates a high-speed, on-chip clock, eliminating the need for an external clock source. CLK_{CTR} allows external control of the clock frequency (f_{CLK}) and, thus, the resolution. The divided CLK signal, CLK_{DIV}, drives the controller.

The proposed system employs an I-DAC current scaling method to improve the system's robustness over widely varying optical path and luminophore conditions. Fig.4 shows the IC system's timing diagram. The system begins in an "Idle" state, with V_{PD} reset to V_{REF}. After the "Idle" state, the LED turns ON while other components remain idle, allowing the luminescence response of the CO_2 sensor to settle in 10-15 μs. The system then enters the "Count1" state, where the I-DAC is at full capacity. The counter records current injections, with the final count, CNT1', representing the area under the I_{PD} curve (A1), equivalent to the total emission from CO_2-sensitive and reference luminophores. In the "Count2" state, the I-DAC again operates at full capacity, with CNT2' reflecting the decay curve area of the reference luminophores (A2). The system then returns to the"Idle" state, ending the cycle. In subsequent cycles, to scale the I-DAC current, DAC_{BIT} for the "Count1" and "Count2" state is adjusted based on CNT1' and CNT2' from the previous cycle. This current scaling improves the conversion accuracy without requiring multiple comparators, reducing area and power overhead.

IV. Measurement Results

To evaluate the performance of C2D, we injected current to the node V_{PD} using an external I-DAC. Fig.5.a (top) shows the measured resolution at different f_{CLK} with V_{BIAS1} fixed at 1.3 V. Increasing f_{CLK} improves resolution, achieving 0.15 nA/cnt at 320 MHz. Across frequencies, the maximum measurable current is limited to 8 μA, determined by the I-DAC capacity. Fig.5.a (bottom) shows the expanded current range with varying V_{BIAS1} at 320 MHz; lowering V_{BIAS1} to 1.15 V extends the range beyond 30 μA but reduces resolution to 0.63 nA/cnt due to increased current from a single unit I-DAC. However, adjusting f_{CLK} and V_{BIAS1} allows resolution and range customization to fit different optical parts, such as LEDs and PDs, with varying power and responsivity. We then measured the counter output at a constant V_{BIAS1} and f_{CLK} both with and without current scaling, as demonstrated in Fig.5.b. For this test, the current was injected for five times longer during the CNT1 window compared to the CNT2 window, resulting in an expected LR of 5. Fig.5.c demonstrates that the proposed current scaling method enhances conversion accuracy, achieving a mean system error of less than 0.5%.

The testbench setup and results from the PCO_2 sweep experiment are shown in Fig.6.a and b. The CO_2 sensor, placed inside a gas vessel, was exposed to PCO_2 levels from 0 to 76 mmHg. A mass-flow controller (MFC) sets PCO_2 in the vessel, which was increased by 3.8 mmHg per step, with the LR measured at LED optical excitation powers of 45 μW and 95 μW. This experiment is designed to imitate the changes in the PD current under the same PCO_2 conditions. The difference in

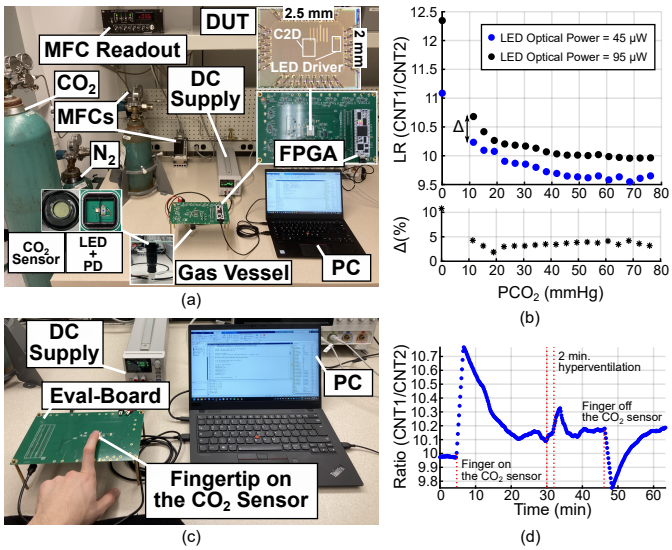

Fig. 6. (a) Gas chamber setup and (b) characterization results, (c) human subject test setup and (d) hyperventilation test results.

LRs between ∼2X optical power levels was about 4% across the entire PCO_2 range, reported in Fig. 6.b, indicating that the t-DLR algorithm minimizes the impact of confounding factors compared to intensity-based methods. Fig.6.c and d detail the setup and results of the human subject test. The test began by measuring atmospheric PCO_2, ∼0 mmHg. After 5 minutes, the subject's finger was placed on the CO_2 sensor. Initially, the LR spiked due to the sudden volume change but soon stabilized as the CO_2 sensor detected CO_2 diffusing from the fingertip. The subject then performed a 2-minute hyperventilation, lowering CO_2 and increasing the LR, which then returned to baseline. Then, the finger was removed, and the LR returned to the atmospheric levels. Both the CO_2 sweep and human subject experiment validate the system's PCO_2 monitoring capabilities.

Table I shows that, to the best of our knowledge, we present the first IC implementation for transcutaneous CO_2 monitoring with the t-DLR method. The resolution of 3.8 mmHg is the best among existing wearables transcutaneous CO_2 monitors within the clinically significant range of 0-76 mmHg. Additionally, the clinically relevant range for O_2 partial pressure, typically 50–150 mmHg, is significantly broader than that of CO_2. This difference in pressure ranges should be noted when comparing O_2 and CO_2 sensor designs and performance requirements.

V. Conclusion

We have presented, to the best of our knowledge, the first integrated circuit implementation of the time-domain dual lifetime referencing technique for measuring the luminescence response of a CO_2-sensitive film, targeting the emerging application of remote and continuous transcutaneous CO_2 monitoring. Our design successfully measured PCO_2 within a range relevant to humans, showing significantly less sensitivity to variations in excitation strength compared to intensity-based approaches. This capability opens new avenues for integrating CO_2 monitoring into future wearable healthcare platforms.

TABLE I
Comparison Table

Parameters	[7] 2023	[5] 2021	[13] 2020	[14] 2022	This Work
Publisher	TBioCAS	Sensors	ISSCC	ESSCIRC	ESSERC
Sensor					
Sensor Type	CO_2	CO_2	O_2	O_2	CO_2
LED (λ)[a]	470 nm	IR	460 nm	450 nm	470 nm
PD (λ)[a]	505/600 nm	IR	618 nm	650 nm	505/600 nm
Hardware					
Technology	PCB	PCB	65 nm	180 nm	180 nm
Chip Area	NA	NA	3.84 mm^2	1.7 mm^2	5 mm^2
Readout	Lum. Ratio	IR	Phase	Lum.	Lum. Ratio
Technique			Luminometry	Lifetime	
Supply Volt.(V)	5	3.3	1.2	1.8	1.8
Power Comp.(μW)	30100	3400	140	835	88[b]
Sampling Rate(SPS)	NR	NR	360	5 M	320 M[c]
Input Range(μA)	NR	NR	NR	NR	30[d]
Resolution(nA/cnt)	NA	NA	NA	NA	0.15[e]
Application					
Sensing Range(mmHg)	0-76	0-38	3.8-150.5[f]	0-228[f]	0-76
Resolution(mmHg)	5	5.25	0.684[g]	<2.2	3.8
Human/Animal Testing	Yes	Yes	No	Yes	Yes

PCB: Printed Circuit Board, NA: Not Applicable, NR: Not Reported, a: Peak wavelength, b: During 1% duty cycle operation, c: Maximum, d: Maximum tested, adjustable, e: Minimum tested, adjustable, f: The range of $PtcO_2$ in humans is (50-150 mmHg) is greater than that of $PtcCO_2$, f: at 3.8 mmHg.

References

[1] A. Umeda *et al.*, "Recent Insights into the Measurement of Carbon Dioxide Concentrations for Clinical Practice in Respiratory Medicine," *Sensors*, vol. 21, no. 16, p. 5636, Aug. 2021.

[2] M. Dicembrino *et al.*, "End-tidal CO_2 and transcutaneous CO_2: Are we ready to replace arterial CO_2 in awake children?" *Pediatric Pulmonology*, vol. 56, no. 2, pp. 486–494, 2021.

[3] W. van Weteringen *et al.*, "Validation of a New Transcutaneous $tcPO_2$/$tcPCO_2$ Sensor with an Optical Oxygen Measurement in Preterm Neonates," *Neonatology*, vol. 117, no. 5, pp. 628–636, 2020.

[4] T. B. Tufan *et al.*, "Implementation Techniques for Transcutaneous Carbon Dioxide Monitoring: Approaches for Wearable Smart Health Applications," *IEEE TBME*, vol. 71, no. 3, pp. 929–943, Mar. 2024.

[5] V. V. Tipparaju *et al.*, "Wearable Transcutaneous CO2 Monitor Based on Miniaturized Nondispersive Infrared Sensor," *IEEE Sensors Journal*, pp. 17 327–17 334, 2021.

[6] T. B. Tufan *et al.*, "An Infra-Red-Based Prototype for a Miniaturized Transcutaneous Carbon Dioxide Monitor," in *2021 IEEE EMBC*, Nov. 2021, pp. 7132–7135.

[7] T. B. Tufan *et al.*, "A Transcutaneous Carbon Dioxide Monitor Based on Time-Domain Dual Lifetime Referencing," *IEEE TBioCAS*, vol. 17, no. 4, pp. 795–807, Aug. 2023.

[8] I. Klimant *et al.*, "Dual Lifetime Referencing (DLR) — a New Scheme for Converting Fluorescence Intensity into a Frequency-Domain or Time-Domain Information," *New Trends in Fluoresc. Spectrosc.: Applications to Chemical and Life Sciences*, pp. 257–274, 2001.

[9] I. Costanzo *et al.*, "Fluorescent intensity and lifetime measurement of platinum-porphyrin film for determining the sensitivity of transcutaneous oxygen sensor," in *IEEE ISCAS*, 2020, pp. 1–5.

[10] I. Costanzo *et al.*, "An Integrated Readout Circuit for a Transcutaneous Oxygen Sensing Wearable Device," in *2020 IEEE CICC*, Mar. 2020.

[11] I. Costanzo *et al.*, "A Nonuniform Sampling Lifetime Estimation Technique for Luminescent Oxygen Measurements for Biomedical Applications," *IEEE JSSC*, pp. 1–15, 2024.

[12] "Cutaneous Carbon Dioxide (PcCO2) and Oxygen (PcO2) Monitors - Class II Special Controls Guidance Document for Industry and FDA," Dec. 2002.

[13] S. Sonmezoglu *et al.*, "34.4 A 4.5mm ^{3} Deep-Tissue Ultrasonic Implantable Luminescence Oxygen Sensor," in *2020 IEEE ISSCC*, Feb. 2020, pp. 454–456.

[14] I. Costanzo *et al.*, "A Nonuniform Sampling Lifetime Estimation Technique for Luminescent Oxygen Measurements," in *2022 IEEE ESSCIRC*, Sep. 2022, pp. 413–416.